

Elastic and inelastic scattering studies for the systems $^{12}\text{C} + ^{28}\text{Si}$ and $^{16}\text{O} + ^{28,29,30}\text{Si}$

P. Braun-Munzinger, G. M. Berkowitz, M. Gai,* C. M. Jachcinski,† T. R. Renner, and C. D. Uhlhorn‡

Department of Physics, State University of New York, Stony Brook, New York 11794

J. Barrette and M. J. LeVine

Brookhaven National Laboratory, Upton, New York 11973

(Received 29 September 1980)

Elastic and inelastic excitation functions for the systems $^{12}\text{C} + ^{28}\text{Si}$ and $^{16}\text{O} + ^{28,29,30}\text{Si}$ have been measured at $\theta_{\text{c.m.}} = 180^\circ$ from the Coulomb barrier up to $E_{\text{c.m.}} = 45$ MeV ($^{12}\text{C} + ^{28}\text{Si}$), $E_{\text{c.m.}} = 52$ MeV ($^{16}\text{O} + ^{28}\text{Si}$), and $E_{\text{c.m.}} = 32$ MeV ($^{16}\text{O} + ^{29,30}\text{Si}$). Over the whole energy range they all exhibit pronounced and regular broad oscillations ($0.5 \lesssim \theta \lesssim 1.5$ MeV). Elastic and inelastic angular distributions up to $\theta_{\text{c.m.}} = 180^\circ$ were taken at five of the maxima and near a minimum of the excitation function for the system $^{16}\text{O} + ^{28}\text{Si}$. All angular distributions are oscillatory and exhibit a strong backward rise. The data are discussed in terms of a coherent superposition of a background and a resonant amplitude and in terms of the interference between the internal and barrier wave reflected by a deep optical potential.

NUCLEAR REACTIONS $^{12}\text{C} + ^{28}\text{Si}$, $^{16}\text{O} + ^{28}\text{Si}$, $^{16}\text{O} + ^{29}\text{Si}$, $^{16}\text{O} + ^{30}\text{Si}$, measured elastic and inelastic $\sigma(\theta, E)$, $14 \text{ MeV} < E_{\text{c.m.}} < 52 \text{ MeV}$, $15^\circ < \theta_{\text{c.m.}} < 180^\circ$, resonance and optical potential analysis.

I. INTRODUCTION

Since the first observation¹ of unexpectedly large cross sections near $\theta_{\text{c.m.}} = 180^\circ$ for elastic and inelastic scattering between medium heavy nuclei, much experimental effort has been devoted to systematic studies of these and related phenomena. In these subsequent investigations, resonancelike structures of width around $0.5 \lesssim \Gamma \lesssim 1.5$ MeV were found in large angle elastic scattering excitation functions for the systems $^{16}\text{O} + ^{28}\text{Si}$ and $^{12}\text{C} + ^{28}\text{Si}$.^{2,3} Similar and possibly related structures were also observed for the α -transfer reactions $^{24}\text{Mg}(^{16}\text{O}, ^{12}\text{C})^{28}\text{Si}$ (Refs. 4 and 5) and $^{28}\text{Si}(^{16}\text{O}, ^{12}\text{C})^{32}\text{S}$ (Refs. 6 and 7) near $\theta_{\text{c.m.}} = 0^\circ$ and 180° . In addition to these gross structures, a fine structure of width in the range $50 < \Gamma < 300$ keV is observed in many systems^{2,5} and has recently been investigated extensively.⁸

The physical origin of the gross structures is, as yet, not fully understood. Various explanations have been proposed ranging from the occurrence of possibly overlapping shape resonances in the ion-ion potential² and scattering from surface transparent optical potentials⁹⁻¹¹ to more exotic effects like explicit parity dependence of the ion-ion potential.^{12,13} At present, none of these approaches gives a consistent description of all the existing data.

In the present paper, we report on an extensive investigation of elastic and inelastic scattering at large angles for the systems $^{12}\text{C} + ^{28}\text{Si}$ and $^{16}\text{O} + ^{28}\text{Si}$. For both systems, data have been taken over a wide energy range from near the Coulomb

barrier (E_{Coul}) to $E_{\text{c.m.}} \approx 3 \times E_{\text{Coul}}$. Over the whole energy range, excitation functions taken at $\theta_{\text{c.m.}} = 180^\circ$ exhibit pronounced and regular gross structures. Angular distributions taken at five of the maxima and near a minimum in the $^{16}\text{O} + ^{28}\text{Si}$ elastic scattering excitation function all display oscillations at backward angles.

In order to investigate the question of whether the observed structures are due to isolated resonances, we have performed an analysis of the angular distributions in terms of a coherent superposition of a background and a resonance amplitude. Furthermore, using a simple parametrization for the elastic S matrix and the Austern-Blair relation¹⁴ to relate the inelastic to the elastic S matrix, an alternative description of the elastic and inelastic angular distributions has been tried assuming an explicit parity dependence of the elastic scattering amplitude. Comparison between these model predictions should indicate how sensitively such models can be tested on the basis of the measured angular distributions.

For the system $^{16}\text{O} + ^{28}\text{Si}$, the measured data are sufficiently complete so that one might hope to be able to put constraints on the underlying ion-ion potential. As has already been demonstrated,^{2,3,5} the sequence of dominant angular momenta deduced from the elastic scattering angular distributions are clearly not compatible with the predictions of a simple shape resonance model in which the standing waves all have the same principal quantum number. Therefore, shape resonances similar to those invoked for the interpretation of $^{16}\text{O} + ^{16}\text{O}$ elastic scattering¹⁵ can only be responsible for the

observed structures if the ion-ion potential is sufficiently attractive ($V_0 < -50$ MeV) to allow the "grazing" trajectory to intersect several closely spaced Regge trajectories.²

As has been shown by Lee,¹⁰ optical model calculations using such deep potentials produce structures in the $\theta_{c.m.} = 180^\circ$ excitation function which are qualitatively similar to those observed in the data even if the absorptive strength used in the calculations is sufficiently large for all shape resonances to overlap. In order to check the predictions of this model more quantitatively, we have performed calculations of angular distributions and excitation functions using an *S*-matrix parametrization suggested by Lee^{10,16} and based on the semiclassical analysis of his optical model calculations. The question to be answered by such a calculation is whether an optical model based description of the backward angle excitation function may be successful in describing the observed structures, especially if the radial shape of the underlying optical potential is not restricted to a Woods-Saxon shape, as has been successfully tried in the analysis of elastic α -particle scattering.¹⁷ Fairly strong indications that the "resonancelike" structure observed in backward-angle elastic and forward angle transfer reactions are not caused by *isolated* resonances has emerged from detailed studies of channel-channel cross correlations between elastic and inelastic scattering and transfer reactions.^{6,18} In these analyses, a high degree of correlation is only found between elastic and inelastic scattering, while the correlations between the α -transfer reaction and elastic scattering in the corresponding entrance and exit channels is generally very weak. Furthermore, from a detailed Breit-Wigner analysis of angular distributions for the reaction $^{24}\text{Mg}(^{16}\text{O}, ^{12}\text{C})$ it was found¹⁹ that at some energies, at least two resonances contribute to the cross section.

In order to obtain information on the dependence of the enhanced backward angle scattering on the neutron number of the target or projectile, we have also performed studies of the excitation functions for the systems $^{16}\text{O} + ^{29,30}\text{Si}$. In contrast to measurements for the systems $^9\text{Be} + ^{28}\text{Si}$, $^{13}\text{C} + ^{28}\text{Si}$,²⁰ and $^{18}\text{O} + ^{28}\text{Si}$ (Ref. 21), cross sections near $\theta_{c.m.} = 180^\circ$ for $^{16}\text{O} + ^{29,30}\text{Si}$ are only reduced by a factor of ~ 5 from those observed for $^{16}\text{O} + ^{28}\text{Si}$. Furthermore, the gross structures found in their excitation function are very similar, suggesting a dynamical rather than structural origin of the observed phenomena.

After a description, in Sec. II, of the experimental methods used to obtain the data, the results of the measurements are presented in Sec. III.²² The analysis of the data in terms of the various models

is described in Sec. IV. Section V contains a discussion of the neutron excess dependence.

II. EXPERIMENTAL METHOD

The elastic and inelastic scattering angular distributions for the systems $^{16}\text{O} + ^{28,30}\text{Si}$ at angles $\theta_{c.m.} \lesssim 100^\circ$ were obtained using the ^{16}O beams of the State University of New York at Stony Brook FN tandem Van de Graaff facility. For these measurements natural SiO and enriched $^{30}\text{SiO}_2$ targets of 50–100 $\mu\text{g}/\text{cm}^2$ thickness were used. The forward angle angular distributions were measured using silicon surface barrier detectors, with the exception of the data at $E_{c.m.} = 34.8$ MeV, where the data in the range $20 \lesssim \theta_{c.m.} \lesssim 150^\circ$ were obtained with standard ΔE - E surface barrier detector telescopes. Data at large center of mass angles were obtained using the $^{28,29,30}\text{Si}$ beams from the Brookhaven National Laboratory MP tandem Van de Graaff accelerators. The angular distribution at large center of mass angles and the $\theta_{c.m.} = 180^\circ$ excitation functions were obtained by detecting the recoiling ^{16}O or ^{12}C ions in a 60 cm long dual wire proportional counter placed in the focal plane of the Brookhaven quadrupole-dipole-dipole-dipole (QDDD) spectrometer. Particle identification was obtained by measuring the specific energy loss, energy, and position along the focal plane of the ions. By kinematically reversing the reaction, i.e., using silicon as a projectile and detecting the recoiling ^{12}C or ^{16}O ions at forward laboratory angles, the recoiling ions have high energies and can be easily detected. Furthermore, in reversing the reaction, the ratio between the solid angle in the center of mass and laboratory system is considerably enhanced; this is particularly important at intermediate angles where the cross section is small and the kinematic broadening ($dE/d\theta$) is large. Typical spectra measured in this way are seen in Fig. 1. The energy resolution is completely determined by the target thickness and reflects the difference in energy loss between the projectile and recoil ions in the target. Self-supporting Al_2O_3 targets of 50–200 $\mu\text{g}/\text{cm}^2$ thickness and ^{12}C targets of 50–100 $\mu\text{g}/\text{cm}^2$ thickness were used. For normalization purposes a 5 $\mu\text{g}/\text{cm}^2$ thick gold layer was evaporated on some of the targets. As seen in Fig. 1, a complete separation of the elastic and inelastic peaks was always possible. At or near $\theta_{lab} = 0^\circ$ the identification of the recoiling ions is more difficult due to the degeneracy that often exists between the $^{16}\text{O}(8^+)$ and $^{12}\text{C}(6^+)$ recoiling ions and one of the charge states of the projectile. The projectile component was moved off the focal plane by placing a Ni foil in front of the entrance slits of the spectrometer. The difference in energy loss

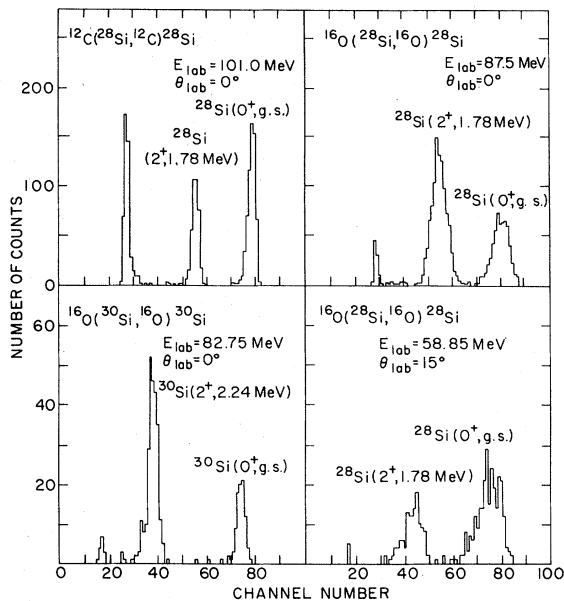


FIG. 1. Energy spectra for the reactions $^{12}\text{C}(^{28}\text{Si}, ^{12}\text{C})^{28}\text{Si}$, $^{16}\text{O}(^{28}\text{Si}, ^{16}\text{O})^{28}\text{Si}$, and $^{16}\text{O}(^{30}\text{Si}, ^{16}\text{O})^{30}\text{Si}$ obtained at and near $\theta_{\text{lab}} = 0^\circ$ with the QDDD spectrometer. The peak at the left end of the spectra is due to the inelastic excitation of higher excited states and it extends beyond the edge of the focal plane detector.

between the beam and recoiling ^{16}O and ^{12}C ions removed the degeneracy so that no appreciable background is observed even at $\theta_{\text{lab}} = 0^\circ$ (see Fig. 1). The energy spread caused by the energy loss straggling of the recoil ions in this additional foil is a negligible contribution to the overall energy resolution.

The data in the angular range $100 \leq \theta_{\text{c.m.}} \leq 150^\circ$ for the angular distribution at $E_{\text{c.m.}} = 22.7$ and 24.1 MeV were measured using a position sensitive parallel plate avalanche counter (PPAC) placed at the entrance of the QDDD spectrometer. A mask in front of the PPAC permitted simultaneous measurements at four angles separated by 1° in the laboratory. A cross section of the PPAC is shown in Fig. 2. Two unsupported foils of $\sim 100 \mu\text{g}/\text{cm}^2$ polypropylene served as pressure foils. In between, two highly parallel, stretched foils of $\sim 75 \mu\text{g}/\text{cm}^2$ polypropylene served as supports for the conductive material of the cathode and anode. A gold film of approximately $40 \mu\text{g}/\text{cm}^2$ thickness was sputtered on one foil in 1 mm strips separated by 0.5 mm to serve as cathode. A gold coated foil of comparable thickness served as the anode. Each strip of the cathode was connected to one tap of a delay line. The position of the avalanche discharge caused by a passing ion was then determined by the centroid of the charge distribution induced on the nearby cathode strips. The delay between the

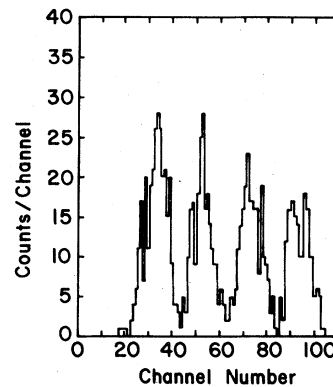
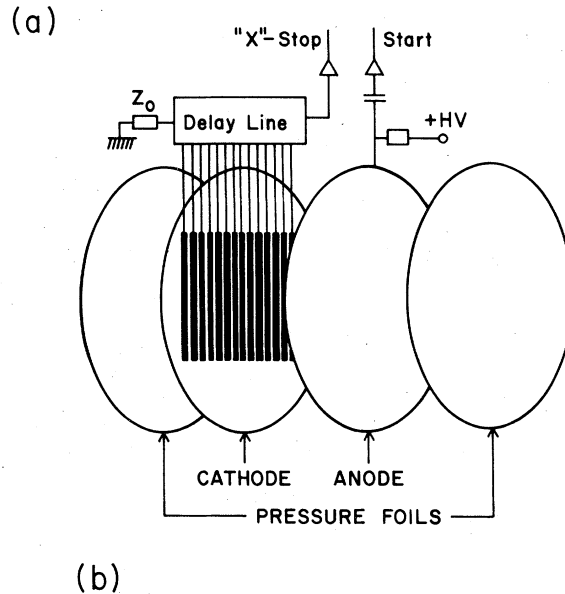


FIG. 2. (a) Schematic view of the parallel plate avalanche counter used in connection with the QDDD spectrometer. (b) Angular resolution obtained with this device for the reaction $^{16}\text{O}(^{28}\text{Si}, ^{16}\text{O})^{28}\text{Si}$. Each peak is separated by $\theta_{\text{lab}} = 1^\circ$.

strips is adjusted to optimize counting-rate capabilities or position resolution. In the present experiment a delay of 10 ns between adjacent strips was used to produce a position resolution of less than 1 mm with greater than 98% detection efficiency at a counting rate of 30 kHz. With *n*-heptane gas at approximately 5 Torr the total areal density of the detector was $\sim 500 \mu\text{g}/\text{cm}^2$.

The measurement of the $\theta_{\text{c.m.}} = 180^\circ$ ($\theta_{\text{lab}} = 0^\circ$) excitation functions was done using a horizontal and vertical aperture of $\Delta\Omega = 80 \times 100$ (mrad)². Due to the decrease in the difference of the range for the beam particles and recoiling ions, the excitation

functions below $E_{c.m.} = 21$ MeV for the systems $^{16}\text{O} + ^{28,29,30}\text{Si}$ were measured at $\theta_{c.m.} = 175.4^\circ$ ($\theta_{lab} = 2.3^\circ$) with an aperture of $\Delta\Omega = 30 \times 100$ (mrad)². This has little effect on the shape of the excitation function since at these low energies, the angular distributions do not vary appreciably in the angular range $175 < \theta_{c.m.} < 180^\circ$.

Relative cross sections were obtained by normalizing to two monitor detectors placed symmetrically on either side of the beam. The absolute normalization of the angular distributions at forward angles ($\theta_{c.m.} \lesssim 100^\circ$) was obtained by measuring at far forward angles where the cross section follows the Rutherford law. The uncertainty in this range is believed to be $\pm 15\%$. Relative normalization of the angular distributions at large angles obtained with the spectrometer were corrected for the charge state distribution of the outgoing ions. The charge state distribution was measured at several angles for each angular distribution and interpolated at the other angles. Results were found to agree within 10% with the predicted distributions of Ref. 23. The absolute normalization of the backward angles data was determined both from the overlap with the forward angle near $\theta_{c.m.} = 100^\circ$ and by detecting ^{28}Si ions elastically scattered from ^{16}O at far forward angles whenever possible. The uncertainty in the absolute cross section is estimated to be $\pm 30\%$ except for the angular distribution at $E_{c.m.} = 34.8$ MeV, where data in the range $90^\circ \lesssim \theta_{c.m.} \lesssim 150^\circ$ and $150^\circ \lesssim \theta_{c.m.} \lesssim 180^\circ$ were obtained with two different setups,¹ increasing the uncertainty for the data at the largest angles ($150 \lesssim \theta_{c.m.} \lesssim 180^\circ$) to $\pm 50\%$.

The relative normalization of the excitation functions was obtained by monitoring the ions scattered from a thin gold layer evaporated onto the targets. Measurements were repeated at many energies to check for possible changes in the target thickness. The charge state distribution was also determined at several energies and the data were corrected accordingly at all energies. For the systems $^{16}\text{O} + ^{28,29,30}\text{Si}$ the absolute normalization was done assuming that the cross section at the lowest energies follows the Rutherford law. For the system $^{12}\text{C} + ^{28}\text{Si}$, the absolute cross sections were obtained by normalizing to the Rutherford elastic scattering of ^{28}Si by the ^{12}C target at $E_{c.m.} = 22.5$ MeV over the laboratory range from 5° to 12° . The error on the absolute scale is estimated to be $\pm 25\%$.

Since most angular distributions were measured with relatively thin targets ($\approx 50 \mu\text{g}/\text{cm}^2$) the energy averaging over the fine structure⁸ is less than for the excitation functions where thicker targets ($\approx 100 \mu\text{g}/\text{cm}^2$) were used. This and the large angular averaging used in the measurement of the excitation functions make for large uncertainties

in any comparison of the absolute cross section of the angular distribution and excitation function data. These considerations may explain the discrepancy of roughly a factor of 2 between the normalization of the angular distributions and excitation functions at $E_{c.m.} = 34.8$ MeV apparent, for example, from a comparison of Figs. 4 and 7. All center of mass energies have been corrected for the energy loss in the targets.

III. EXPERIMENTAL RESULTS

Excitation functions measured at $\theta_{c.m.} = 180^\circ$ for elastic and inelastic scattering of $^{12}\text{C} + ^{28}\text{Si}$ and $^{16}\text{O} + ^{28}\text{Si}$ are presented in Figs. 3 and 4. Part of these excitation functions have been published previously.² In both channels of the two reactions, the cross sections are dominated by a series of regularly spaced structures with large peak to valley ratios and widths of $\Gamma \approx 1-5$ MeV. However, there are also qualitative differences between the two systems. For example, in the case of $^{16}\text{O} + ^{28}\text{Si}$ the envelope of the cross section drops between 20 and 36 MeV but then increases fairly dramatically to a maximum near $E_{c.m.} = 46$ MeV. At energies $E_{c.m.} > 50$ MeV the structures seem to disappear altogether. This is in contrast to the data for $^{12}\text{C} + ^{28}\text{Si}$, where the envelope of the cross section is nearly constant over the whole energy range and a disappearance of the structures at the upper end of the energy range is not as obvious. The maximum at $E_{c.m.} = 46$ MeV for the system $^{16}\text{O} + ^{28}\text{Si}$ is all the more surprising if compared to available

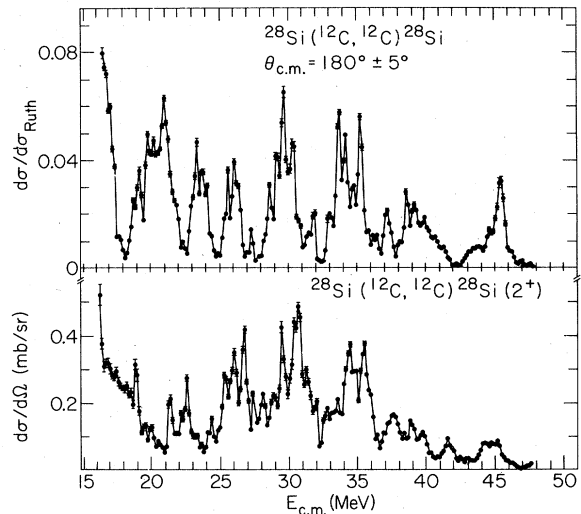


FIG. 3. Excitation functions for elastic and inelastic scattering of $^{12}\text{C} + ^{28}\text{Si}$ measured at $\theta_{c.m.} = 180^\circ$. The solid angle used in this measurement was $\Delta\Omega = (80 \times 100)$ (mrad)². Vertical bars represent the statistical error only.

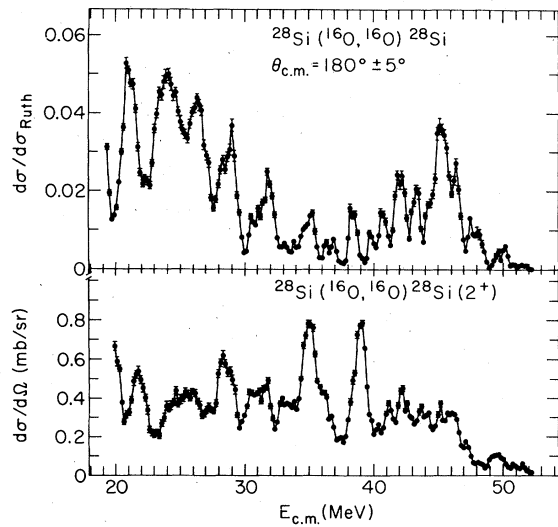


FIG. 4. Excitation function for elastic and inelastic scattering of $^{16}\text{O}+^{28}\text{Si}$ measured at $\theta_{c.m.} = 180^\circ$. The solid angle in this measurement was $\Delta\Omega = (80 \times 100)(\text{mrad})^2$. Vertical bars represent the statistical error only.

forward angle data. The measured forward angle cross section²⁴ at this energy drops exponentially, without exhibiting oscillations, to a value of $d\sigma/d\sigma_{\text{Ruth}} < 5.10^{-4}$ at $\theta_{c.m.} = 60^\circ$. Yet, from the $\theta_{c.m.} = 180^\circ$ excitation function, $d\sigma/d\sigma_{\text{Ruth}} \sim 0.04$ at $E_{c.m.} \approx 46$ MeV (see Fig. 4), which corresponds to $d\sigma/d\sigma_{\text{Ruth}}(180^\circ) \sim 0.08$ after correcting for the averaging due to the large solid angle used in the excitation function measurements. The present data, therefore, correspond to a backward rise of many orders of magnitude. It is also interesting to note that the widths and the spacings of the structures do not seem to increase with increasing bombarding energy.

It is especially obvious for the system $^{12}\text{C}+^{28}\text{Si}$ that each of the gross structures is fragmented, exhibiting a finer structure of width $50 < \Gamma < 300$ keV. This is also true for the system $^{16}\text{O}+^{28}\text{Si}$, but not visible in Fig. 4 because of energy averaging in the target. Detailed measurements and analyses of these finer structures have been reported elsewhere.⁸ Since, in the present paper, the focus is on the gross structures, the measured excitation functions have been computer-averaged using a running Gaussian average with widths of 0.8 and 0.91 MeV for $^{12}\text{C}+^{28}\text{Si}$ and $^{16}\text{O}+^{28}\text{Si}$, respectively. These energy averaged excitation functions are shown in Figs. 5 and 6. This procedure, in addition to emphasizing the regularity of the structures, also demonstrates the high degree of correlation between elastic and inelastic scattering, especially for the case of $^{16}\text{O}+^{28}\text{Si}$.

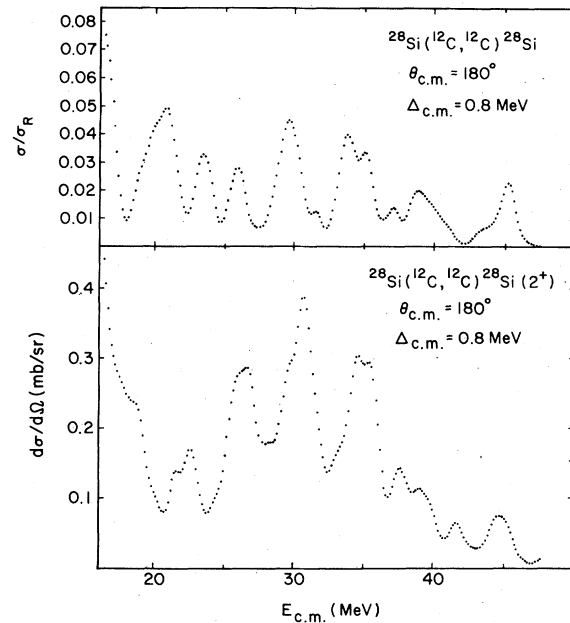


FIG. 5. Computer averaged excitation functions at $\theta_{c.m.} = 180^\circ$ for $^{12}\text{C}+^{28}\text{Si}$. The averaging interval is $\Delta_{c.m.} = 0.8$ MeV.

For the system $^{16}\text{O}+^{28}\text{Si}$, extensive angular distributions have been measured at five maxima and near a minimum of the elastic excitation function. The data for the elastic scattering angular distributions are shown in Fig. 7. All angular distributions are strongly oscillatory, even the one near a minimum of the excitation function. This is in contrast to measured angular distributions

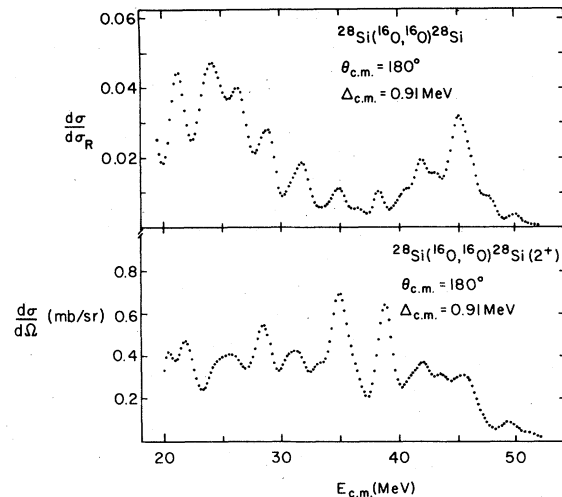


FIG. 6. Computer averaged excitation functions at $\theta_{c.m.} = 180^\circ$ for $^{16}\text{O}+^{28}\text{Si}$. The averaging interval is $\Delta_{c.m.} = 0.91$ MeV.

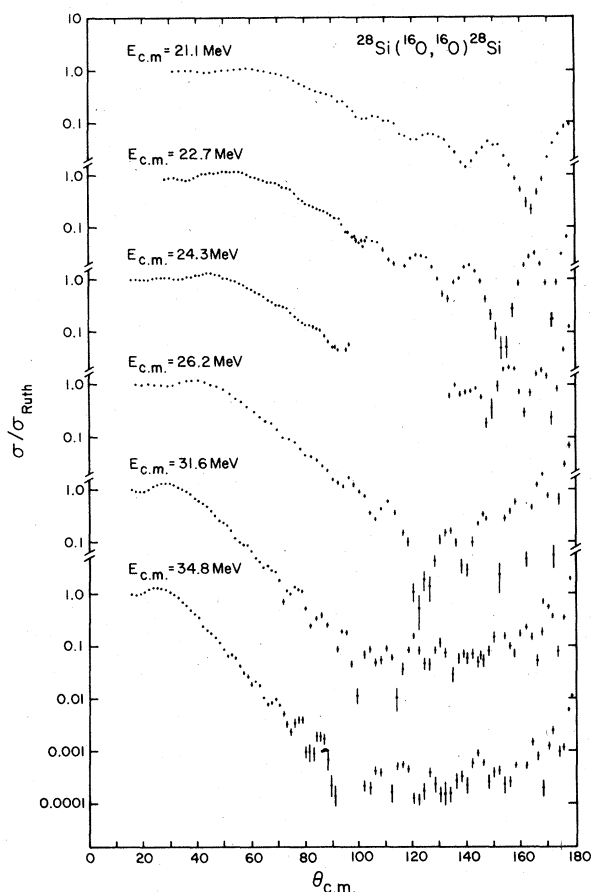


FIG. 7. Elastic scattering angular distributions for the system $^{16}\text{O} + ^{28}\text{Si}$. All data have been taken at energies corresponding to maxima in the excitation function except for the distribution at $E_{c.m.} = 22.7$ MeV, which is near a minimum.

for the system $^{12}\text{C} + ^{28}\text{Si}$,³ where it was reported that "off-resonance" angular distributions generally are flat and structureless. For the higher energies, $E_{c.m.} > 24$ MeV, the backward angle part exhibits oscillations very similar to those predicted by the square of a single Legendre polynomial. The envelope of the angular distributions exhibits a very strong backward rise which follows, or is even steeper than, the $1/\sin\theta$ envelope of the square of a single Legendre polynomial. Measured angular distributions for the inelastic scattering to the first excited state in ^{28}Si ($E^* = 1.78$ MeV, $J = 2^+$) are presented in Fig. 8. While the angular distribution measured at the lowest energy ($E_{c.m.} = 21.1$ MeV) is fairly structureless, the angular distributions get increasingly oscillatory at the higher energies with a pronounced rise towards backward angles. An interesting feature of these angular distributions is that they all have a relative

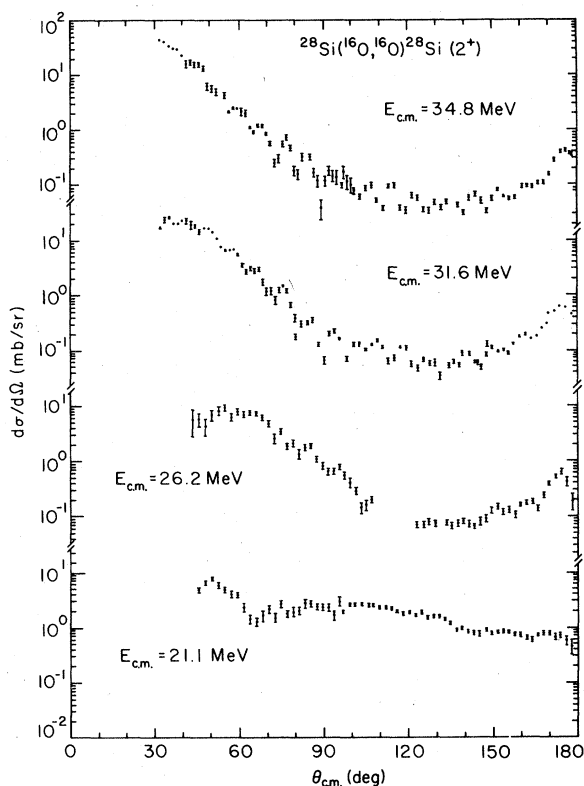


FIG. 8. Angular distributions for the inelastic scattering to the first excited state in ^{28}Si ($E^* = 1.78$ MeV, $J = 2^+$).

minimum at $\theta_{c.m.} = 180^\circ$. If we describe the reaction in a coordinate system in which the quantization axis is chosen along the beam direction, then the relative minimum at $\theta_{c.m.} = 180^\circ$ shows that magnetic substates with $m \neq 0$ are dominantly populated in the inelastic reaction since at $\theta_{c.m.} = 180^\circ$, only $m = 0$ components of the scattering amplitude can contribute.

In Fig. 9, excitation functions at $\theta_{c.m.} = 180^\circ$ (or near 180° ; see Sec. II) are compared for the systems $^{16}\text{O} + ^{28,29,30}\text{Si}$ in the energy range $14 < E_{c.m.} < 33$ MeV. These data show that the resonancelike structures observed for $^{12}\text{C} + ^{28}\text{Si}$ and $^{16}\text{O} + ^{28}\text{Si}$ are not confined to α -like systems, but rather are only moderately damped by the addition of one or two neutrons to the ^{28}Si nucleus. The spacings and widths of the structures for $^{16}\text{O} + ^{29,30}\text{Si}$ are, indeed, very similar to those observed for $^{16}\text{O} + ^{28}\text{Si}$. This behavior of the cross section at large angles appears to be a fairly general phenomenon and suggests a common reaction mechanism.

In the following sections, various models proposed for understanding the present data are investigated with special emphasis on the question

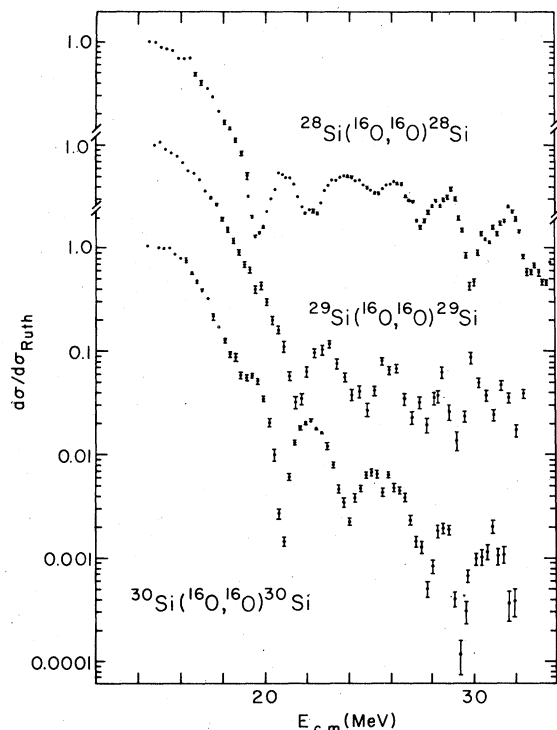


FIG. 9. Comparison of elastic scattering excitation functions at $\theta_{c.m.} = 180^\circ$ for the systems $^{16}\text{O} + ^{28,29,30}\text{Si}$.

of whether the reported structures are due to isolated resonances or caused by a dynamic mechanism in the ion-ion potential. The analysis concentrates entirely on the $^{16}\text{O} + ^{28}\text{Si}$ system since complete angular distributions exist only for this system and the qualitative features of the excitation functions for the system $^{12}\text{C} + ^{28}\text{Si}$ are very similar to those for the system $^{16}\text{O} + ^{28}\text{Si}$.

IV. ANALYSIS OF THE DATA

A. Isolated resonances

In order to assess the possibility that the observed structures correspond to isolated states in the composite system ($A=44$ for $^{16}\text{O} + ^{28}\text{Si}$), we have performed a simple resonance analysis of the measured angular distributions. For elastic scattering of spinless particles, the scattering amplitude is expanded in partial waves

$$f(\theta) = f_{\text{Coul}}(\theta) + \frac{1}{2ik} \sum (2l+1) e^{2i\sigma_l} (S_l - 1) P_l(\cos\theta). \quad (1)$$

In our analysis, the nuclear part of the S -matrix element, S_l , is composed of a background and a resonant part

$$S_l = S_l^0 + S_l^R \cdot \delta_{l,J_R}, \quad (2)$$

where the background S -matrix S_l^0 is obtained from an optical model calculation using a strongly absorbing potential. The resonance part is assumed to have a Breit-Wigner energy dependence

$$S_{J_R}^R = -ie^{2i\delta_{J_R}^0} \frac{De^{2i\phi}}{E - E_R + i\Gamma/2}, \quad (3)$$

where $\delta_{J_R}^0$ is the nuclear background phase, D and Γ are the partial and total width, respectively, and ϕ is a "resonance mixing phase." In the present investigation, the choice of the optical model potential generating the background S -matrix elements was dictated by the requirement that all standing wave resonances be sufficiently wide so that the cross section as a function of energy is smooth. For simplicity, we have chosen the potential $E18$ of Ref. 24, which is very strongly absorbing and fulfills the above condition. At backward angles, calculations using this optical potential generally underestimate the measured cross sections by several orders of magnitude.¹

In Fig. 10 the results of these optical model and resonance calculations are compared to the measured angular distributions for five energies corresponding to maxima in the excitation function. For these calculations the resonance mixing phase ϕ was fixed at 0° . It is clear from this figure that the resonance parametrization accounts for the salient features observed in the angular distributions, especially at backward angles, though the middle angle region ($100 \leq \theta_{c.m.} \leq 140^\circ$) is usually not as well reproduced. The spin values quoted in Table I are uncertain to $\pm 1\hbar$, due mainly to the uncertainty in the background amplitude at low energy and to the angular and statistical uncertainties in the data at high energy.

"On resonance" the calculated angular distributions mainly depend on the ratio D/Γ which is fixed by the cross section near 180° . An interesting result of the above calculations is that the ratio D/Γ depends nearly exponentially on energy, as shown in Table I. In a resonance interpretation of the present data one may speculate that, since Γ is essentially energy independent (see Figs. 5 and 6), the partial elastic width exhausts a smaller and smaller fraction of the total width as energy, and, therefore, the number of open channels, increases.

In order to find out whether the angular distribution measured at $E_{c.m.} = 22.7$ MeV, i.e., between two maxima of the excitation function, can also be described by the resonance parametrization, we have performed a set of calculations using a background S matrix plus two resonances at $E_R^{(1)} = 21.1$ MeV with $J_R^{(1)} = 9^-$, and $E_R^{(2)} = 24.1$ MeV with $J_R^{(2)} = 16^+$.

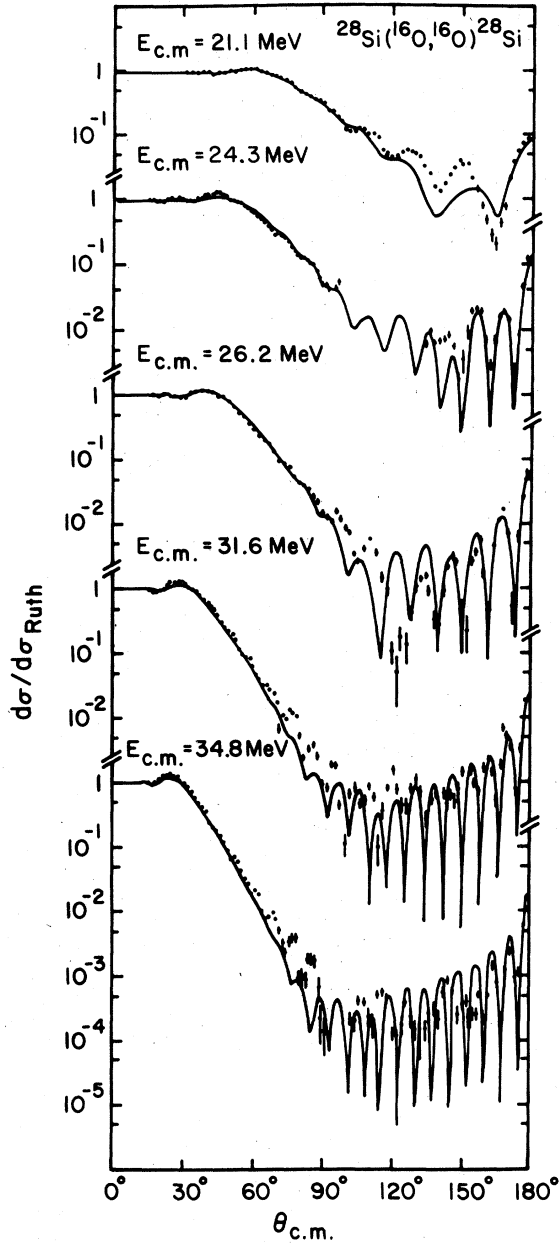


FIG. 10. Optical model plus resonance calculations for the system $^{16}\text{O} + ^{28}\text{Si}$ assuming a resonance mixing phase $= 0^\circ$. For further details, see text and Table I.

The "spins" of these resonances, the values of D/Γ , and the resonance mixing phase ϕ were fixed from their experimental widths and by fitting the measured angular distributions at 21.1 and 24.1 MeV as well as the excitation function in this energy region. For this analysis one has, of course, to take proper account of the energy dependence of the partial elastic width D . In R -matrix theory,

TABLE I. Single resonance parameters used for the calculation of the angular distributions presented in Fig. 10.

$E_{c.m.}$ (MeV)	J_R	D/Γ
21.1	9	0.077
24.1	16	0.070
26.2	16	0.048
31.6	22	0.020
34.8	24	0.016

this energy dependence can be expressed in terms of the penetrability P and reduced width γ_{red} for the state, i.e.,

$$D = 2 \cdot P \cdot \gamma_{red}^2, \quad (4a)$$

where P is written in terms of the regular and irregular Coulomb wave functions as

$$P = \frac{KR}{F_{J_R}^2 + G_{J_R}^2}. \quad (4b)$$

Since the spin values J_R are always close to the grazing angular momentum, P normally varies quite strongly with energy. In principle, the level shift and the energy dependence of the total width Γ should also be taken into account. In the present calculations, the former quantity was found to be quite small compared to the total width and, therefore, of little influence on the results. The energy dependence of Γ was neglected in the present work, mainly because it involves a sum over many open channels and cannot easily be estimated. Furthermore, it has been shown in a similar analysis (see Ref. 19) that an energy dependence of Γ equal to that of D has negligible influence on the results. If this resonance model is correct, then the above parameters completely determine the angular distributions at all energies between $E_R^{(1)}$ and $E_R^{(2)}$, and therefore, the angular distribution at 22.7 MeV should be correctly predicted. The results of these calculations are shown in Fig. 11. The spin values, reduced widths, and total widths used are presented in Table II. Surprisingly, although the angular distributions at the maxima of the excitation function are again, as in Fig. 10, rather well reproduced, the shape of the angular distribution at 22.7 MeV is not well fitted by these calculations. The situation does not improve if the spin values for the two resonances are changed by ± 1 unit of \hbar . Therefore, the oscillatory shape of the angular distribution at $E_{c.m.} = 22.7$ MeV is probably *not* caused by interference between two resonances. It should, however, be noted that the assumed background cross section is about an order of magnitude smaller than the measured cross section at the minimum of the excitation function;

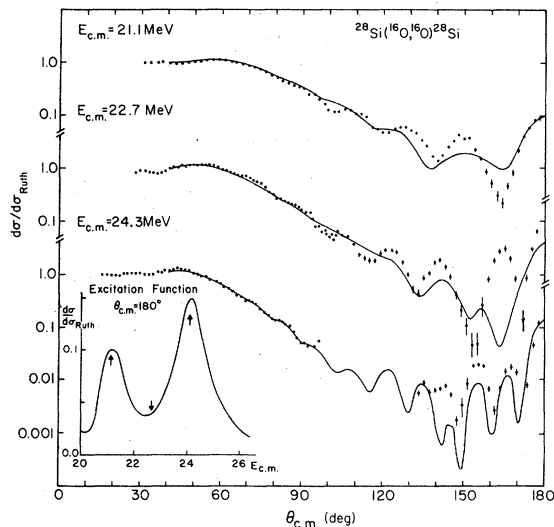


FIG. 11. Two level resonance analyses of the elastic scattering angular distributions corresponding to the peaks at $E_{c.m.} = 21$ and 24.1 MeV and near a minimum in between. The insert shows the excitation function predicted by this calculation and the positions (arrows) of the measured angular distributions.

consequently, the calculations are very insensitive to details of the background amplitude. This situation could, of course, be drastically changed if a different, less strongly absorbing potential is used to generate the background.

Summarizing the results of the optical model + resonance calculations, one finds that while the angular distributions at or near the maxima of the excitation function can be successfully described using such a parametrization, the angular distribution near a minimum is not well described by this procedure. This casts some doubt on the interpretation of the data in terms of isolated resonances. Furthermore, the spin sequence obtained by these calculations is fairly irregular (see Table I) and completely excludes an interpretation of the present data in terms of a single rotational band.

B. Parity dependent optical model

It was shown in Ref. 12 that introducing an empirical parity dependence into the optical model potential yields a good description of the low energy part of the $\theta_{c.m.} = 180^\circ$ excitation function and also predicts reasonably well some of the measured angular distributions. Partly due to the large numbers of free parameters, attempts have not been made to improve on the description given in Ref. 12. Rather, in this section, we want to discuss very briefly a simple parametrization including a parity dependence and apply this to a description of both elastic and inelastic scattering. In this

TABLE II. Parameters used in the two resonances plus background calculations shown in Fig. 11.

$E_{c.m.}$ (MeV)	J_R	$\gamma_{red}^{elastic}$ ($\text{MeV}^{1/2}$)	Γ (MeV)	ϕ
21.1	9	5.5×10^{-2}	1.0	0°
24.1	16	6.5×10^{-2}	1.6	0°

model, the nuclear part of the elastic S matrix is written as

$$S_l = S_l^0 + 2iA(-)^l \cdot f(l), \quad (5a)$$

where, for simplicity, the form factor $f(l)$ is parametrized in terms of the background S-matrix S^0 via

$$f(l) = |S_l^0| (1 - |S_l^0|). \quad (5b)$$

In addition to S_l^0 , the only adjustable parameter is then the amplitude A . The calculations using this parametrization illustrate that once the elastic scattering cross section is reproduced, there is essentially no new information on the dynamics of the reaction necessary to describe the inelastic scattering over the full angular range. To demonstrate this we have, for simplicity, computed S_l^0 in terms of the diffraction model of Frahn and Venter,²⁵ and adjusted the "background" parameters²⁶ to reproduce the forward angle part of the elastic scattering cross section. Adding a parity dependent amplitude of $A=0.01$ then yields elastic cross sections which fairly well describe the measured data (see Fig. 12). Using the elastic S-matrix elements obtained in this way, we have computed the cross section for the inelastic scattering $^{28}\text{Si}(^{16}\text{O}, ^{16}\text{O})^{28}\text{Si}^*(2^+, 1.78 \text{ MeV})$ in the Austern-Blair approximation.¹⁴ The results of these calculations are shown in Fig. 13. It is surprising how well this simple model describes the data, even including the minimum at $\theta_{c.m.} = 180^\circ$. This result illustrates that except for the deformation length, the inelastic scattering does not contain more information on the reaction mechanism than elastic scattering, even if the cross sections are known over the full angular range $30 \leq \theta_{c.m.} \leq 180^\circ$.

It should be noted that in the calculation of Ref. 12 the optical model potential used is very weakly absorbing. In fact, near $E_{c.m.} = 21$ MeV, the central depth of the imaginary potential is only 1.4 MeV so that effects from potential resonances, especially for the surface partial waves, should be important. Furthermore, the frequency of the oscillations observed in the angular distributions at 26.2, 24.1, and 22.7 MeV is not well reproduced by these calculations, indicating the possible need for a modification of the optical model potential. Lastly, as explained in the following section, a deep opti-

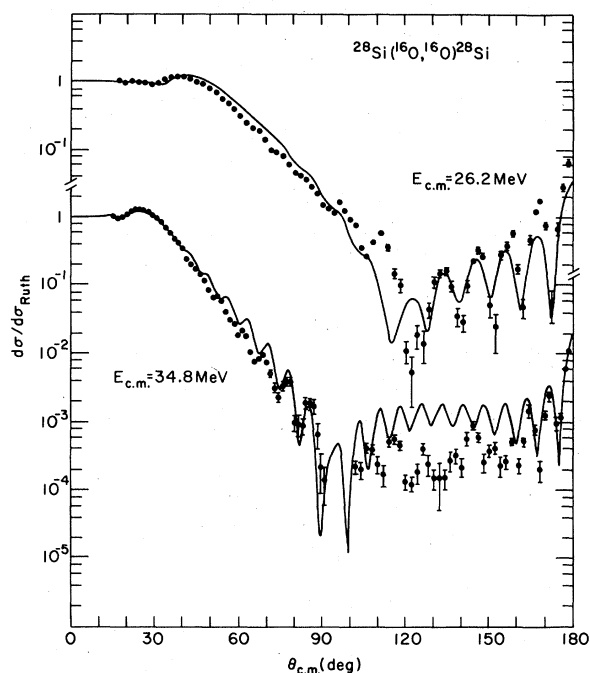


FIG. 12. Strong absorption plus parity dependence calculations compared to $^{16}\text{O} + ^{28}\text{Si}$ elastic scattering angular distributions. For details, see text.

cal model potential may generate an S matrix similar to that produced by the above model without explicitly introducing a parity dependent term into the optical model potential.

C. Interference between internal wave and barrier wave

From a semiclassical analysis of optical model calculations it has been shown²⁷⁻²⁹ that for most optical potentials the nuclear part of the elastic S matrix can be separated into two parts:

$$S = \eta_i^B + \eta_i^I, \quad (6)$$

corresponding to reflection of the incident wave at the external barrier (η^B) and single or multiple reflection from the interior of the potential (η^I). The interference between the barrier wave and the internal wave then gives rise to characteristic structures in angular distributions and excitation functions. For example, it can be shown [see Eq. (4.6) in Ref. 27] that for a nuclear potential $V_n(r)$ which is nearly constant in the internal region, the difference between the phase δ_i^B of the barrier wave and the phase δ_i^I of the internal wave is linear in angular momentum with a slope near $-\pi/2$, i.e.,

$$2(\delta_i^B - \delta_i^I) \approx -\pi \cdot l + f(E), \quad (7)$$

where $f(E)$ is a function of energy to be discussed

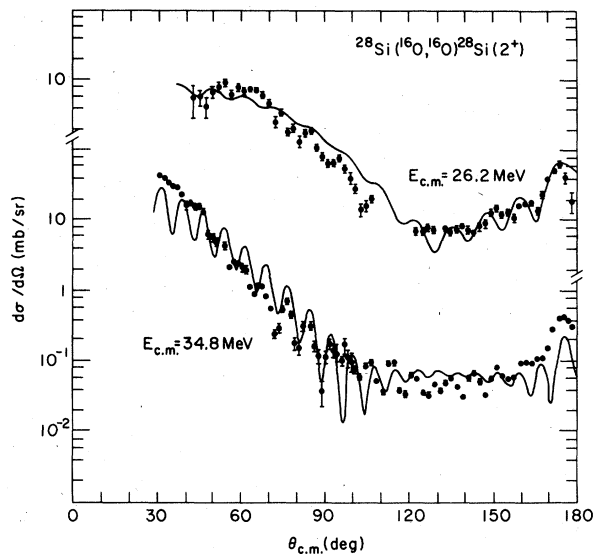


FIG. 13. Predictions of the strong absorption plus parity dependence parametrization for the inelastic scattering of $^{16}\text{O} + ^{28}\text{Si}$, using the Austern-Blair approximation.

below. Using Eq. (7), the S matrix can be approximated by¹⁶

$$S_l \approx \eta_i^B \left[1 + \frac{|\eta_i^I| (-)^l e^{if(E)}}{|\eta_i^B|} \right]. \quad (8)$$

As can be seen, this phase difference introduces an even-odd staggering in the S matrix similar to the one obtained by explicitly introducing a parity dependence into the potential. Furthermore, using this result, it has been shown¹⁰ that the energy spacing of structures in the $\theta_{c.m.} = 180^\circ$ excitation function caused by the interference between the internal wave and the barrier wave is roughly given by

$$\Delta E \approx 2/(dl_{gr}/dE), \quad (9)$$

where l_{gr} is the grazing angular momentum. This simple estimate agrees relatively well with our measured data. Optical model calculations¹⁰ with a choice of parameters guided by the above considerations indeed produced structures similar to those observed in the $\theta_{c.m.} = 180^\circ$ excitation function. However, the peak to valley ratio of the structures is generally too small and strongly decreases for increasing energy, contrary to what is observed in the data (see Fig. 4). These results are interesting enough to warrant further investigation of this model. Rather than trying to improve on Lee's optical potential,¹⁰ we have started from the simple parametrizations for the barrier and internal wave given in Refs. 10 and 16. Using these prescriptions, the barrier wave S matrix

is approximated by Ericson's parametrization,^{30,31} i.e.,

$$\eta_I^B = [1 + e^{-i\gamma_B} e^{(l_{gr}-1)/\Delta_B}]^{-1}. \quad (10)$$

Similarly, the magnitude of the internal wave is written as

$$\eta_I^I = \eta_0^I \cdot [1 + e^{i\gamma_I} e^{(l_{gr}-1)/\Delta_I}]^{-1}. \quad (11)$$

Semiclassical considerations predict $\Delta_B = 2\Delta_I$, so the parameters involved in Eqs. (10) and (11) are l_{gr} , γ_B , γ_I , Δ_B , and η_0^I . The value of l_{gr} is fixed by optical model calculations using strongly absorbing potentials; γ_I and γ_B have been set equal to $\pi/2$ (all results are insensitive to the specific choice of this angle) and Δ_B has been fixed at $\Delta_B = 1.15$, which is consistent with the predictions of optical model calculations. The magnitude of the internal wave, of course, depends on the amount of absorption present and has been chosen to decrease exponentially with energy, i.e., $\eta_0^I = C_3 e^{-C_4 E_{c.m.}}$. From a fit to the envelope of the $\theta_{c.m.} = 180^\circ$ cross section the parameters C_3 and C_4 were fixed to be 4 and 0.17, respectively. For the phase difference between the internal wave and the barrier wave we have used Eq. (7) and approximated $f(E)$ by $f(E) = C_1 + C_2 \cdot E_{c.m.}$. The parameters C_1 and C_2 are not free, but are intimately connected to the shape resonances in the underlying optical model potential. At each energy corresponding to a shape resonance, the internal and barrier wave interfere destructively,

$$\delta_I^I - \delta_I^B = (n + \frac{1}{2}) \cdot \pi, \quad (12)$$

where n is the principal quantum number of the resonance. Of course, since the absorption is not very weak, these shape resonances are not isolated but strongly overlapping as indicated by the small value of η_0^I .^{10,16} Yet, dynamically, only those shape resonances whose energy and angular momentum lie close to the grazing trajectory, will contribute to the cross section. This point has already been proposed in Ref. 2 as a possible explanation of the backward scattering anomalies. Therefore, a specific choice of C_1 and C_2 corresponds to a trajectory of shape resonances in the ion-ion potential. For potentials of the class used by Lee¹⁰ one finds that C_2 varies smoothly from 1.2 to 0.4 as the energy increases from $E_{c.m.} = 20$ to 40 MeV. (The parameter C_1 just fixes the overall phase of the structure near 180° and is relatively unimportant.) Using parameters in this range, a series of calculations of excitation functions and angular distributions were performed for the system $^{16}\text{O} + ^{28}\text{Si}$. Typical results are shown in Figs. 14 and 15. It is obvious from these figures that many aspects of the data are well reproduced by the calculations. The peak to valley ratio and the frequency of the oscil-

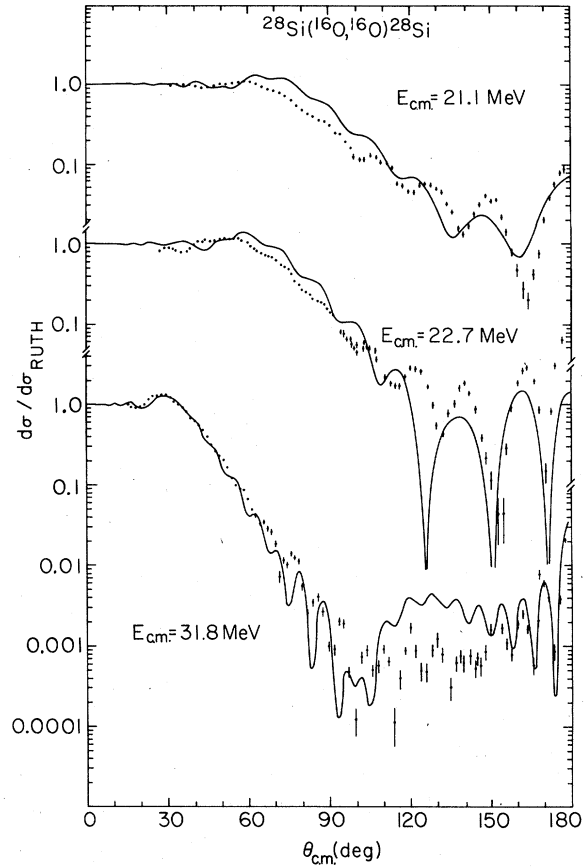


FIG. 14. Comparison of elastic scattering angular distributions for $^{16}\text{O} + ^{28}\text{Si}$ with the predictions of the barrier-wave-internal-wave interference model as described in the text.

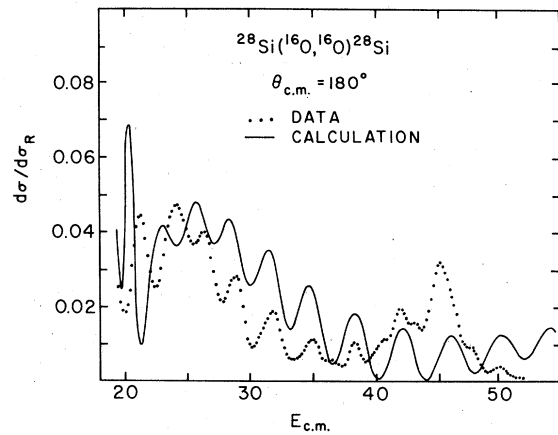


FIG. 15. Comparison of the computer averaged excitation function at $\theta_{c.m.} = 180^\circ$ for $^{16}\text{O} + ^{28}\text{Si}$ (dotted line) with the predictions of the barrier-wave-internal-wave interference model (solid line). The parameters used in the calculation are given in the text.

lations in the excitation function at $\theta_{c.m.} = 180^\circ$ are correctly predicted. A satisfactory fit is also obtained for the angular distributions, as is evidenced in Fig. 14 simultaneously for positions corresponding to maxima and a minimum in the excitation function. It should be noted that even though the calculations do use relatively many parameters, most of them are determined by the semiclassical arguments underlying Eq. (7) and the resonance condition stated in Eq. (12). On the other hand, our results cannot be considered quantitative proof of this model as it is not simple to determine the underlying ion-ion potential from our parametrization. However, the present results indicate clearly that the observed structures at backward angles may be explained by dynamical models without having to resort to the picture of isolated resonances. The interference between barrier and internal waves is an important effect even if the underlying shape resonances are strongly overlapping.

V. NEUTRON EXCESS DEPENDENCE

The data shown in Fig. 9 clearly indicate that the "anomalous" large angle scattering is not restricted to systems consisting of α -particle nuclei but rather persists even if one or two neutrons are added to the heavy partner. The average reduction in cross section is about a factor of 5, but the spacings and width of the structures are very similar to those observed for the system $^{16}\text{O} + ^{28}\text{Si}$. A previous investigation²¹ of the system $^{18}\text{O} + ^{28}\text{Si}$ had revealed a reduction of the elastic cross section near $\theta_{c.m.} = 180^\circ$ by more than two orders of magnitude over the one observed for the system $^{16}\text{O} + ^{28}\text{Si}$. This large difference might be due to the fact that in ^{18}O the two additional neutrons occupy a new major shell with a corresponding increase in their rms radius.

The strong structures observed for the systems $^{16}\text{O} + ^{29,30}\text{Si}$ are again very difficult to understand in a description involving isolated shape resonances. In order to reduce the average cross section the absorptive strength W has to be increased. Increasing the absorption, however, invariably increases the width of the structures according to $\Gamma \approx \Gamma_{\text{decay}} + 2W$; consequently, the structures should be very much smeared out for the systems $^{16}\text{O} + ^{29,30}\text{Si}$, a result at variance with our observations. On the other hand, the interference between barrier wave and internal wave explains such an effect quite naturally. In this model, increased absorption could decrease both the cross sections due to the barrier wave and due to the in-

ternal wave, so that the interference pattern may be essentially unchanged.

VI. CONCLUSION

In the present investigation we have shown that the existing data in large angle elastic scattering for systems such as $^{16}\text{O} + ^{28}\text{Si}$ cannot easily be described by models invoking isolated resonances as the cause of the observed broad structures. An explicit parity dependent term in the optical model potential may yield a successful description of the existing data. However, by using semiclassical arguments, it was shown²⁷ that similar l dependences in the nuclear part of the elastic S matrix can also be produced in the optical model without an explicit angular momentum dependent potential. If the real potential is deep and the absorption moderate, the interference between the internal and barrier wave gives rise to structures in angular distributions and excitation functions which are very similar to those observed in the experimental data. If the pocket in the potential disappears, the distinction between the barrier wave and the internal wave is lost. This will result in a reduction of the cross section and the absence of interference effects. Inspection of our data shows that for the system $^{16}\text{O} + ^{28}\text{Si}$, there is indeed a strong decrease of the $\theta_{c.m.} = 180^\circ$ cross section for energies $E_{c.m.} > 45$ MeV (see Fig. 3). It would be very interesting to pursue similar measurements to higher energies. They may provide fairly precise information on the depth of the real part of the interaction potential between heavy ions and would lend further support to the interpretation that for these medium heavy systems, the observed structures are caused by an interference between internal and barrier waves.

The present analysis of the data shows that the peaks observed in the excitation functions cannot be associated with isolated states in the composite system. However, the interference effect described above is closely related to the (overlapping) shape resonances in the ion-ion potential. A mapping of the position of these standing waves could provide otherwise inaccessible information on the interaction between complex nuclei.

ACKNOWLEDGMENTS

The authors acknowledge many stimulating and helpful discussions with S. Y. Lee. This work was supported in part by the National Science Foundation and by the Division of Basic Energy Sciences, U. S. Department of Energy, under Contract No. DE-AC02-76CH00016.

- *Present address: Wright Nuclear Structure Laboratory, Yale University, New Haven, Conn. 06520.
- † Present address: Argonne National Laboratory, Argonne, Ill. 60439.
- ‡ Present address: Institut für Experimentalphysik, Ruhr-Universität, Bochum, West Germany.
- ¹P. Braun-Munzinger, G. M. Berkowitz, T. M. Cormier, J. W. Harris, C. M. Jachcinski, J. Barrette, and M. J. LeVine, *Phys. Rev. Lett.* **38**, 944 (1977).
- ²J. Barrette, M. J. LeVine, P. Braun-Munzinger, G. M. Berkowitz, M. Gai, J. W. Harris, and C. M. Jachcinski, *Phys. Rev. Lett.* **40**, 445 (1978).
- ³M. R. Clover, R. M. DeVries, R. Ost, N. J. A. Rust, R. N. Cherry, Jr., and H. E. Gove, *Phys. Rev. Lett.* **40**, 1008 (1978).
- ⁴M. Paul, S. J. Sanders, J. Cseh, D. F. Geesaman, W. Henning, D. G. Kovar, C. Olmer, and J. P. Schiffer, *Phys. Rev. Lett.* **40**, 1310 (1978).
- ⁵S. M. Lee, J. C. Adloff, P. Chevalier, D. Disdier, V. Rauch, and F. Scheibling, *Phys. Rev. Lett.* **42**, 429 (1979).
- ⁶C. K. Gelbke, T. Awes, U. E. P. Berg, J. Barrette, M. J. LeVine, and P. Braun-Munzinger, *Phys. Rev. Lett.* **41**, 1778 (1978).
- ⁷J. C. Peng, J. V. Maher, M. S. Chiou, W. J. Jordan, F. C. Wang, and M. W. Wu, *Phys. Lett.* **80B**, 35 (1978).
- ⁸J. Barrette, M. J. LeVine, P. Braun-Munzinger, G. M. Berkowitz, M. Gai, J. W. Harris, C. M. Jachcinski, and C. D. Uhlhorn, *Phys. Rev. C* **20**, (1979) 1759.
- ⁹See, e.g., *Proceedings of the Symposium on Heavy Ion Elastic Scattering, Rochester, 1977*, edited by R. M. DeVries (unpublished).
- ¹⁰S. Y. Lee, *Nucl. Phys.* **A311**, (1978) 518.
- ¹¹S. Kahana, B. T. Kim, and M. Mermaz, *Phys. Rev. C* **20**, 2124 (1979).
- ¹²D. Dehnhard, V. Shkolnik, and M. A. Franey, *Phys. Rev. Lett.* **40**, 1549 (1978); M. A. Franey, V. Shkolnik, and D. Dehnhard, *Phys. Lett.* **81B**, 132 (1979).
- ¹³S. Kubono, P. D. Bond, D. Horn, and C. E. Thorn, *Phys. Lett.* **84B**, 408 (1979).
- ¹⁴N. Austern and J. S. Blair, *Ann. Phys. (N. Y.)* **33**, 15 (1965).
- ¹⁵A. Gobbi, R. Wieland, L. Chua, D. Shapira, and D. A. Bromley, *Phys. Rev. C* **7**, 30 (1973).
- ¹⁶S. Y. Lee and Y. H. Chu, report, 1979 (unpublished); S. Y. Lee, Y. H. Chu, and T. T. S. Kuo, report, 1980.
- ¹⁷Th. Delbar, Gh. Gregoire, G. Paic, R. Ceuleneer, F. Michel, R. Vanderpoorten, A. Budzanowski, H. Dabrowski, L. Freindl, K. Grotowski, S. Micek, R. Planeta, A. Strzalowski, and K. A. Eberhard, *Phys. Rev. C* **18**, 1237 (1978).
- ¹⁸M. Paul, S. J. Sanders, D. F. Geesaman, W. Henning, D. G. Kovar, C. Olmer, J. P. Schiffer, J. Barrette, and M. J. LeVine, *Phys. Rev. C* **21**, 1802 (1980).
- ¹⁹S. J. Sanders, M. Paul, J. Cseh, D. F. Geesaman, W. Henning, D. G. Kovar, R. Kozub, C. Olmer, and J. P. Schiffer, *Phys. Rev. C* **21**, 1810 (1980).
- ²⁰R. Ost, M. R. Clover, R. M. DeVries, B. R. Fulton, H. E. Gove, and N. J. Rust, *Phys. Rev. C* **19**, 740 (1979).
- ²¹P. Braun-Munzinger and J. Barrette, *Proceedings of the Symposium on Heavy Ion Elastic Scattering, Rochester, 1977*, edited by R. M. DeVries (unpublished), p. 85.
- ²²See AIP document No. PAPS PRVCA-24-1010-23 for 23 pages of tabulations of the cross sections measured in the present work (and in Ref. 10). Order by PAPS number and journal reference from American Institute of Physics, Physics Auxiliary Publication Service, 335 East 45th Street, New York, N. Y. 10017. The price is \$1.50 for each microfiche (98 pages) or \$5.00 for photocopies of up to 30 pages, with \$.50 for each additional page over 30 pages. Airmail additional. Make checks payable to the American Institute of Physics.
- ²³J. B. Marion and F. C. Young, *Nuclear Reaction Analyses, Graphs and Tables* (North-Holland, Amsterdam, 1968).
- ²⁴J. G. Cramer, R. M. DeVries, D. A. Goldberg, M. S. Zisman, and C. F. Maguire, *Phys. Rev. C* **14**, 2158 (1976).
- ²⁵W. E. Frahn and R. H. Venter, *Ann. Phys. (N. Y.)* **24**, 243 (1963).
- ²⁶In terms of the parameters introduced in Ref. 25, $L_0 = 16.1$, $\mu = 1.5$, and $D = 0.75$ at $E_{c.m.} = 26.2$ MeV and $L_0 = 24.5$, $\mu = 1.5$, and $D = 0.75$ at $E_{c.m.} = 34.5$ MeV. See also R. Anni and L. Taffara, *Rev. Nuovo Cimento* **2**, 1 (1970) for the definition of the parameters.
- ²⁷D. M. Brink and N. Takigawa, *Nucl. Phys.* **A279**, 159 (1977).
- ²⁸N. Takigawa and S. Y. Lee, *Nucl. Phys.* **A292**, 173 (1977).
- ²⁹S. Y. Lee and N. Takigawa, *Nucl. Phys.* **A308**, 189 (1978).
- ³⁰T. E. O. Ericson, in *Preludes in Theoretical Physics* edited by A. de Shalit, H. Feshbach, and L. Van Hove (North-Holland, Amsterdam, 1965), p. 321.
- ³¹For very low energies, $E_{c.m.} \approx E_{Coul}$, this has been replaced by a slightly different parametrization which better reproduces optical model S-matrix elements.